The 12th Hypervelocity Impact Symposium

Scale Size Effect in Momentum Enhancement

James D. Walker[a]*, Sidney Chocron[a], Daniel D. Durda[b], Donald J. Grosch[a], Naor Movshovitz[c], Derek C. Richardson[d], and Erik Asphaug[c].

[a]*Southwest Research Institute, P.O. Drawer 28510, San Antonio, Texas 78228-0510 USA*, [b]*Southwest Research Institute, 1050 Walnut St., Suite 300, Boulder, CO, 80302 USA*, [c]*Department of Earth and Planetary Sciences, University of California at Santa Cruz, Santa Cruz, CA, 95064 USA*, [d]*Department of Astronomy, University of Maryland, College Park, MD, 20742-2421 USA*

Abstract

When an impactor strikes a body at hypervelocities the momentum transferred to the impacted body is greater than the initial impactor momentum. This effect is due to the crater ejecta, and when the impacted body's mass provides some of the momentum change, the effect is referred to as momentum enhancement. The small amount of data on this question implies that there is a scale effect – that is, as the projectile size increases there is an increase in the imparted momentum beyond that anticipated due to the increase in projectile size. Recently, experimental data was gathered on the increase in momentum caused by crater ejecta when 4.45-cm diameter aluminum spheres struck granite targets. The amount of momentum enhancement (characterized by the ratio β) was greater than 2 for 2 km/s impacts. Compared with other data at much smaller scale, these tests imply an impactor scale and an impactor density effect for hypervelocity strikes into rock. The implied impactor size scale effect is surprisingly large – to a 0.4 power – and extrapolation indicates that a 1-meter aluminum sphere striking a consolidated rock surface at 10 km/s could have a β exceeding 40, supposing the scale size effect does not saturate on the order of 10 cm. Such a large momentum enhancement shows that kinetic impactors can be very efficient at deflecting asteroids.

© 2013 The Authors. Published by Elsevier Ltd.
Selection and peer-review under responsibility of the Hypervelocity Impact Society

Keywords: Momentum enhancement, hypervelocity impact, impact experiments, scaling, cratering, failure modeling

1. Recent Experiments

An unknown in asteroid deflection through hypervelocity impact is the quantitative amount of momentum transferred by the impact. With m the mass of the impactor and v the strike speed, the momentum transferred to the struck body is characterized by $\beta = \Delta$momentum$/mv$, where the change in momentum is for the struck object. For hypervelocity impacts, β is greater than 1 and it is thought that the amount of momentum transferred to the impacted asteroid or comet nucleus could be large, on the order of $\beta = 10$ [1]. However, the quantitative uncertainty led to using estimates of β ranging from 1 to 10 in the analyses behind two recent national studies on the topic of mitigating the asteroid impact threat [2-4].

In February 2010 at the Southwest Research Institute ballistic range in San Antonio, Texas, two aluminum spheres of 4.45-cm diameter (124.4 g) were impacted into two 1-meter diameter granite spheres at 2 km/s. Figure 1 shows one of the projectiles and the first granite sphere. Figure 2 shows the effect of the aluminum spheres impacting traditional metal targets at 2 km/s. Figure 3 shows images from the first impact into a 1225 kg granite sphere at 2.01 km/s. The camera frame rate was 6250 frames per second which gives 160 microseconds (μs) between frames. Figure 4 shows some interesting frames from a second test with a 1360 kg granite sphere, including the launching of dust from the back surface of the sphere and the shadow of the shock wave in air from the launch package as it passed over the target at later time

---

* Corresponding author: James Walker. Tel.: (210)522-2051; fax: (210)522-6290.
E-mail address: james.walker@swri.org.

(6 milliseconds). The momentum enhancement was determined by the rocking of the entire stand as it sat on wooden 2×4s. The resulting momentum transferred to the granite spheres was β = 2.13 ± 0.10 and β = 2.22 ± 0.10 for the first and second tests, respectively. The details of the analysis are in Walker, et al. [5] (the IJIE special issue journal publication for this Hypervelocity Impact Symposium). The crater ejecta thrown backwards increases the momentum transferred to the sphere, hence momentum enhancement occurs (i.e., β > 1). The crater extent ranged from 40 to 60 cm. The crater depth at the impact point was roughly 10 cm. The large rock pieces thrown off typically were 2.5 cm thick. Holsapple and Housen [1]

Fig. 1. Images from the experimental set-up: upper left shows the 4.45-cm diameter aluminum sphere with Lexan sabot; upper right shows SwRI's 50-mm powder gun mounted on a rail with x-ray systems (not utilized in these experiments); lower left shows fork lift moving the first test granite sphere; lower right shows the granite sphere on stand on top of wooden 2×4s.
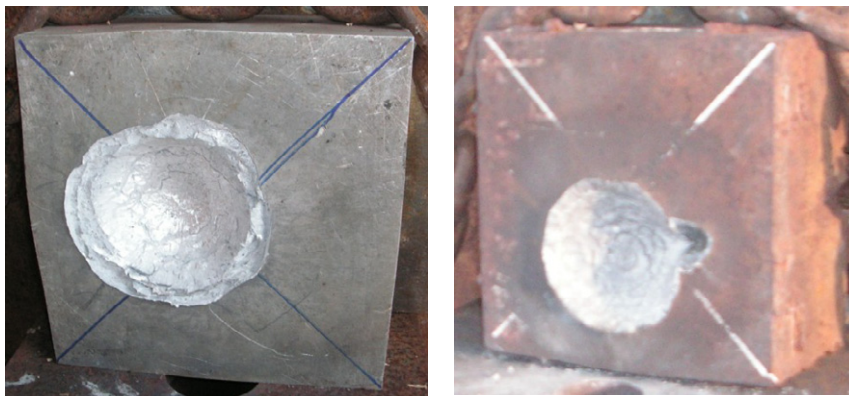

Fig. 2. Impacts of the aluminum spheres into an armor aluminum (left, crater depth 4.1 cm and crater diameter 10 cm) and an armor steel (right; crater depth 1.6 cm and crater diameter 8 cm).
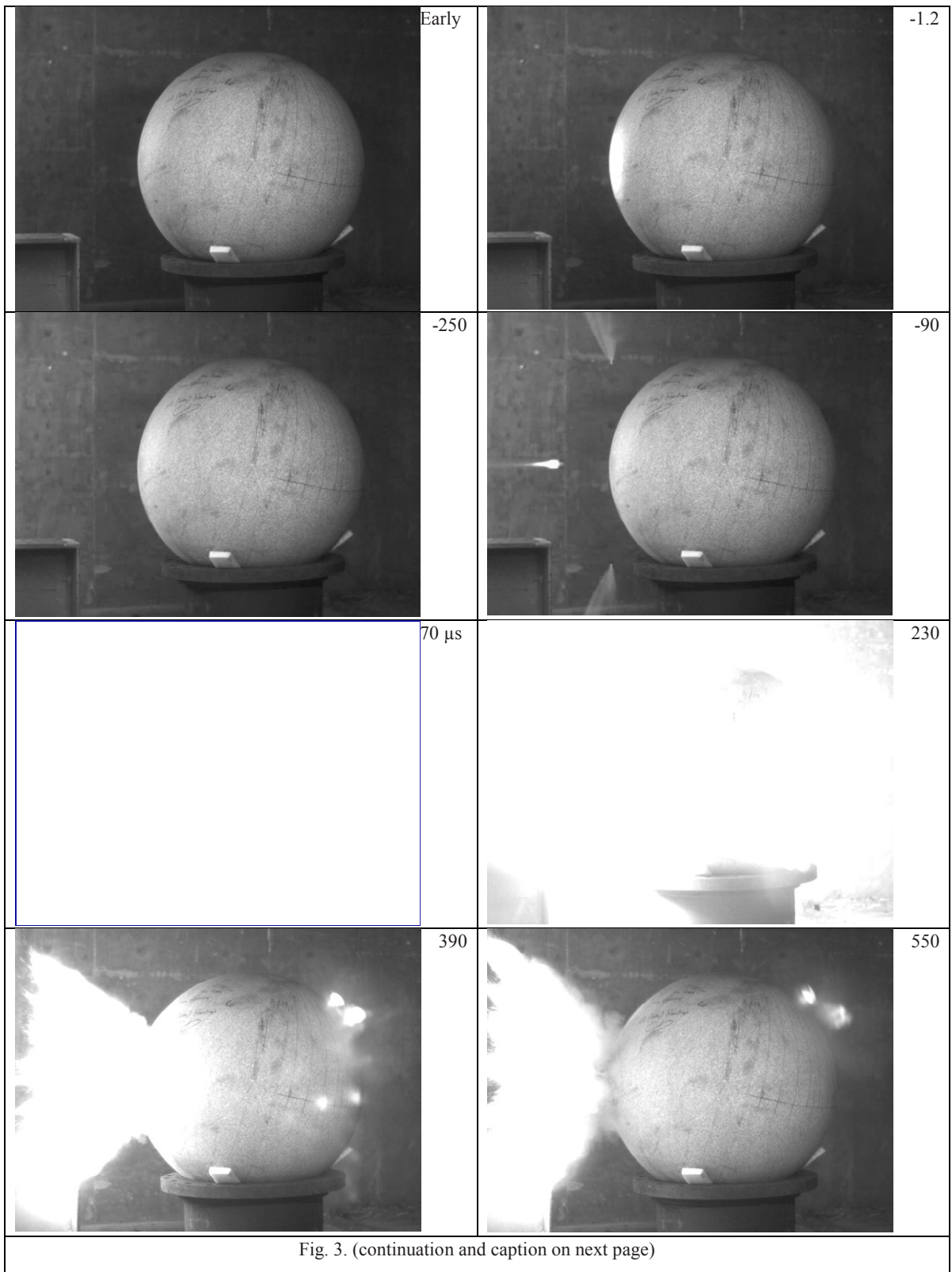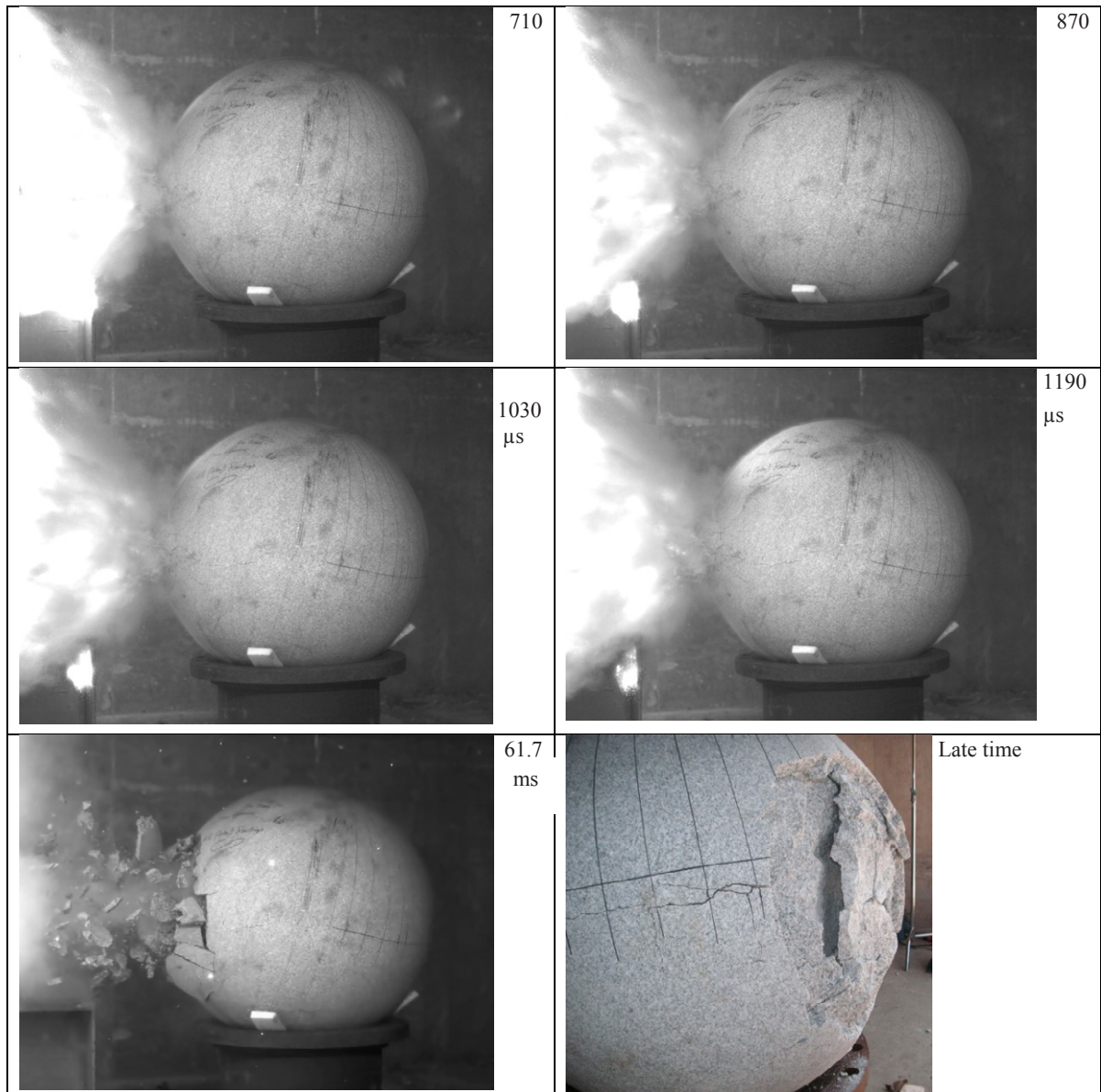
Fig. 3. (continuation and caption on next page)

Fig. 3. Images from the first test. Lighting from the muzzle flash of the granite sphere occurs at 1.2 milliseconds (ms) before impact. The spherical projectile is partially in the frame at 250 microseconds (μs) before the strike. The frame rate is 6250 frames per second, or 160 μs between frames, which corresponds to a flight distance of 32.2 cm between frames. The granite sphere was in shadow and the exposure time was 17 μs. The impact saturates the Phantom camera; subsequent frames show some in-camera flare. Early time debris appears to be ejected in a cone, while late time debris (61.7 ms) of large pieces is primarily heading straight back towards the gun. A post-test image shows a residual bridge of granite within the crater.

present experimental data and computational results on the mass and velocity distribution of crater ejecta material due to impacts. Their analysis implies that the majority of the momentum enhancement comes from low-speed material comprising a large mass. Though they do not report the size of the low-speed fragments, in our tests large, slow pieces are clearly launched in the direction opposite to the impactor flight direction (Fig. 3). Results of CTH computations performed prior to the tests to model the expectations of the impact are in Ref. [5].
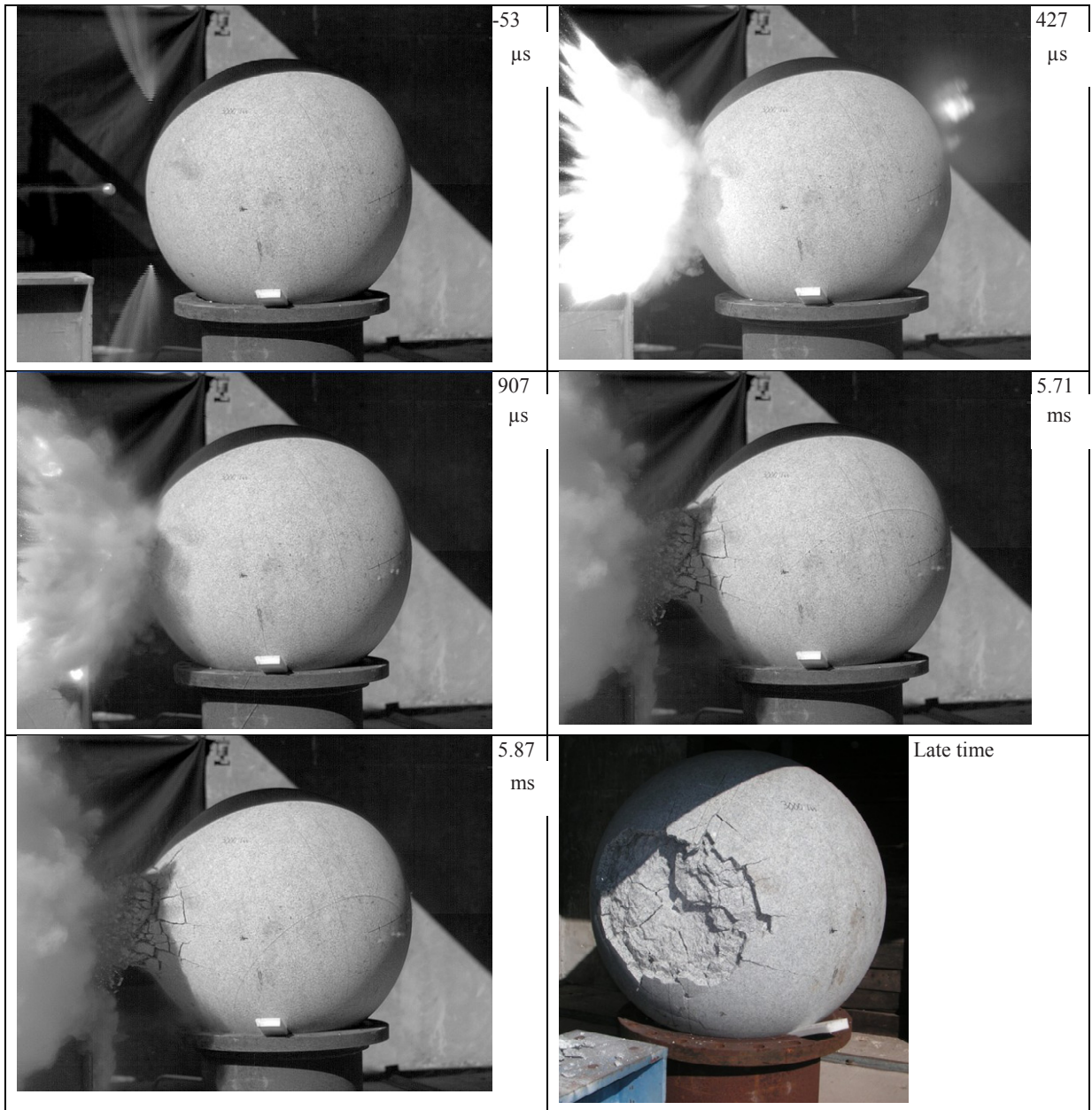
Fig. 4. Selected images from second test. The frame rate was again 6250 frames per second; the sphere sat in direct sunlight and the exposure time was 2 µs. First image shows a vapor trail as spherical aluminum projectile approaches the granite sphere. The next two frames at 427 and 907 µs show dust being launched off the back side of the sphere; for a 5 km/s sound speed in the rock, the expected arrival time is 200 µs after the strike. (Note that the objects in the upper right of the 427 µs image are flare due to bright reflections within the camera; the dust that is being launched is located below the black line near the equator of the sphere.) The next two frames at 5.71 and 5.87 ms show the circular arc of the shock-wave-in-air shadow cast on the target. A late time image shows the final crater.

2. Experimental Data on Momentum Enhancement

To see how these experiments compare to other data for normal or near-normal impact, Fig. 5 shows the results of momentum enhancement experiments into rock with density near 2.7 g/cm^3 [5,6] and aluminums [7,8] with nylon (0.213 gram), polyethylene, and aluminum impactors. The impactors were all spheres, save for a cylinder of polyethylene, and the diameters of the spheres are given in the figures. In our tests the rocking of the test stand was measured to determine momentum enhancement; the rest of experiments measured momentum enhancement using a ballistic pendulum where the target is hung from cables and its post-impact motion is measured. The basalt was identified as having similar density and sound speed as aluminum. Two of the basalt impacts had slight obliquity. The granite also had similar density to aluminum (2.3–2.6 g/cm^3). There are three striking observations from this graph:

1. There is a size scale effect in the aluminum target; i.e., as the size of the impactor increases so does β for the same impact speed.
2. In the aluminum-target impacts, it is clear that the denser impactor produces more momentum enhancement, since all the aluminum impactors (density 2.7 g/cm^3, mass 0.006, 0.0468, 0.373, and 3 grams) weigh less than the polyethylene impactor (density 0.91 g/cm^3, mass 4.1 gram) and the physical sizes of the aluminum impactors are all less than the polyethylene impactors.
3. The weaker aluminum target (1100-O) provides less momentum enhancement than the stronger aluminum target (2024-T4), even though (see below) the craters in the weaker aluminum were larger; however, the ejected mass was less.
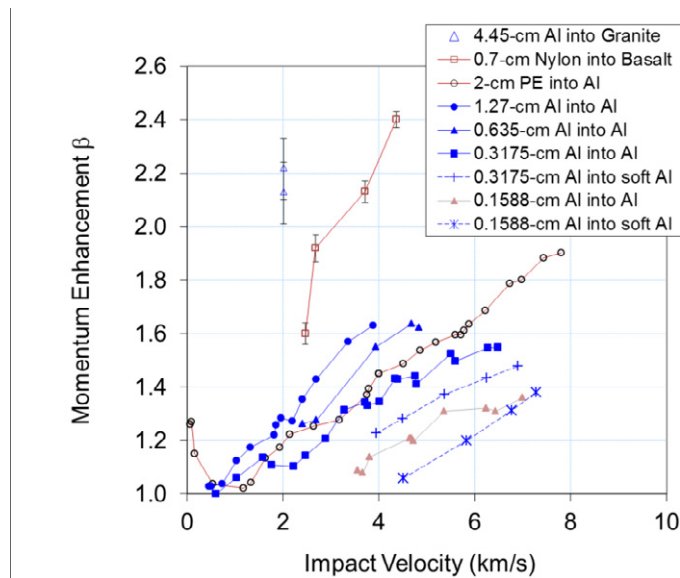

Fig. 5. Experimental results for momentum enhancement β for aluminum spheres striking granite [5], nylon spheres striking basalt [6], polyethylene cylinders striking 2024-T4 aluminum [7], and aluminum spheres striking 2024-T4 aluminum targets [8]. The soft aluminum targets are 1100-O. Impacting aluminum spheres for granite were 6061-T6 and for aluminums were 2017-T4.

To draw conclusions and understand where our data points fit in, we performed analysis of the Denardo and Nysmith data in Ref. [8]. There is a lot of interesting information contained in their report that reveals itself on further analysis. To begin, given that there is a noted size scale effect, one may wonder as to its origins and whether there is enough information in the data to determine the origins. As a first step, note that the depth of penetration and the crater radius do not appear to exhibit a size scale effect. The depth of penetration is reported with respect to the initial undisturbed surface of the target. Figure 6 shows the depth of penetration in terms of projectile diameter and the crater diameter in terms of projectile diameter. Little size scale dependence is in evidence as a function of impact velocity. (Denardo and Nysmith state that the largest size projectile (1.27 cm diameter) shows deeper penetration due to pitting at the bottom of the crater, and when the depth of penetration is determined by estimating a smooth crater bottom without pitting the values are in line with the other scale sizes.) The diameters were measured in multiple directions and then an average was taken. In drawing this little-size-

dependence conclusion is should be kept in mind that as the projectile mass increases, the maximum velocity for which there is data decreases. It is certainly interesting that the crater radius diameter does not show a dependence on the aluminum alloy with its respective strength; the crater depth does, but not the radius. These data points are seen, for the most part, to fall on top of themselves and thus there is little size scale effect in the penetration. As a final plot along these lines, the volume of the crater times the target density normalized by the projectile mass, which essentially provides a normalized mass displaced for the target, is shown (Fig. 7). The figure shows that this displaced mass also does not show a size scale effect, though it does show target-strength dependence. The crater volume was estimated by assuming an ellipsoidal shape with volume = $(\pi/6)P(D_c)^2$.
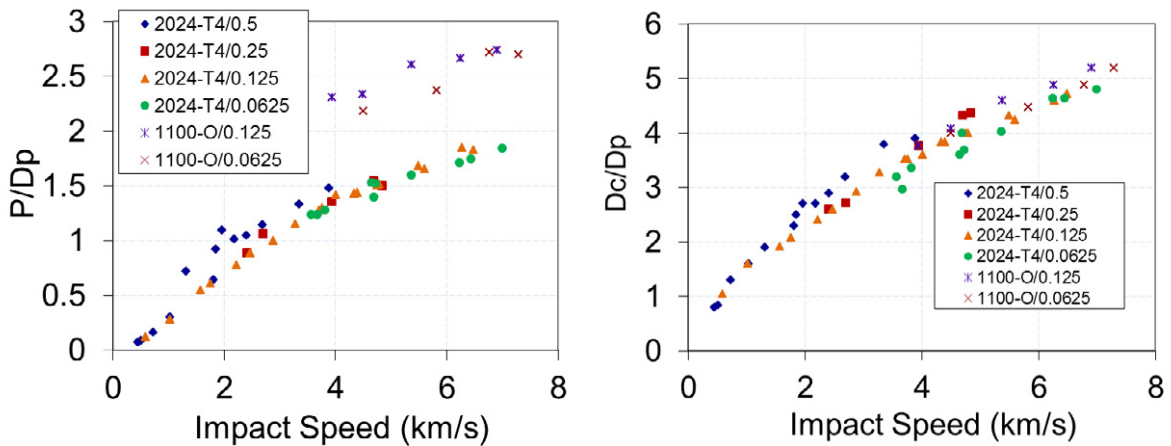

Fig. 6. Crater depth normalized by projectile diameter (left) and crater diameter normalized by projectile diameter (right), both in terms of impact velocity for the aluminum striking aluminum (data from [8]), showing little size scale effect (see text for discussion of the largest projectile size). Legend shows target material alloy/aluminum projectile diameter in inches.
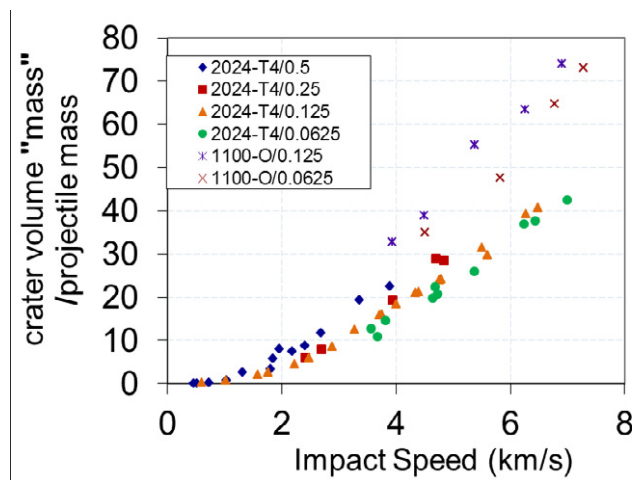

Fig. 7. Displaced mass normalized by projectile mass in terms of impact velocity for the aluminum striking aluminum (data from [8]), showing little size scale effect. Legend shows target material alloy/aluminum projectile diameter in inches.

The "displaced mass" of the crater volume has a number of origins. One is the material pushed radially aside. Another is the material that is pushed into lips that are still attached. Another is the material pushed downward. All these involve material motion for material that is still connected to the target. Part of the crater volume originates from material that failed and is ejected from the target and is no longer connected, which is referred to as the ejecta. Ejecta mass is determined

by the difference of the target plate's mass before and after the test; during the test a plate was placed on the back of the target plate to prevent any spall from that location. How much of the material of the crater volume is ejecta? Figure 8 shows the ejecta mass as a function of impact velocity and shows the ratio of ejecta mass to the mass displaced from the crater volume as a function of impact velocity. There is lots of scatter in this data. However, it appears that for the stronger target (the Al 2024-T4) there is a trend as the projectile size increases that the percentage of the crater volume accounted for by post-test target mass loss (what we are calling ejecta) increases. Denardo and Nysmith looked to see if the effect was due to crater lips detaching as the scale size increased, but that appeared not to be the case. Thus, we might hypothesize that the momentum enhancement effect is due to larger mass ejecta for larger scale size, and that thus there would be a direct correlation between ejecta mass and momentum enhancement. However, when the momentum enhancement β is examined in terms of ejecta mass, it clearly shows an impactor size effect (Fig. 9, left). (However, the right plot in Fig. 9 is intriguing, plotting the momentum enhancement vs. the fraction of the crater volume made up of ejecta material, which does not appear to exhibit a size effect.) The implication of this result is that there is also an ejecta fragment ejection velocity size effect; for example, Denardo [7] measured spray back angles and noted that as the impact velocity increased, the ejecta spray angle decreased: in other words, the ejecta was in more alignment with the shot line than radially away from the shot line as impact velocity increased.
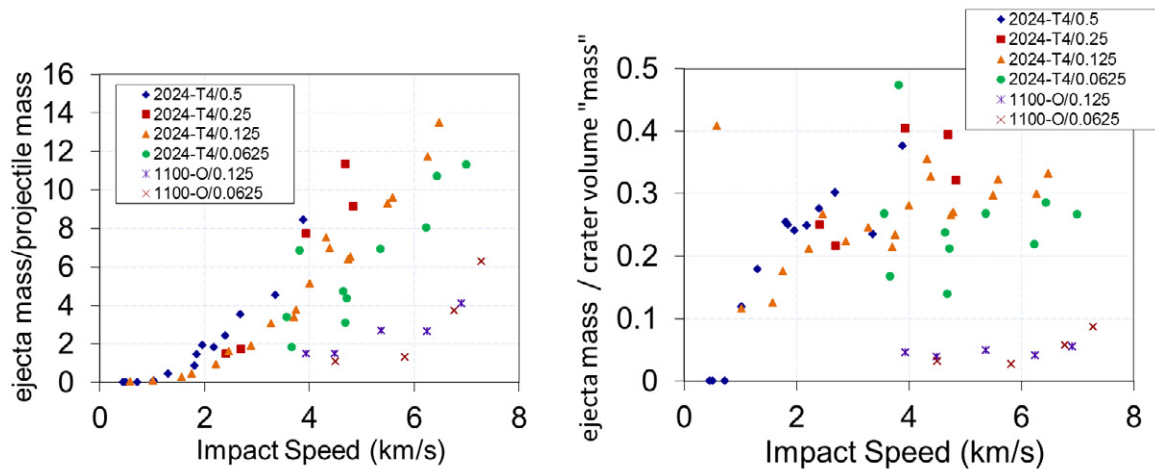

Fig. 8. Ejecta mass normalized by projectile mass (left) and ejecta mass normalized by displaced mass of the crater volume (right), both in terms of impact velocity for the aluminum striking aluminum (data from [8]), showing a size scale effect. Legend shows target material alloy/aluminum projectile diameter in inches.
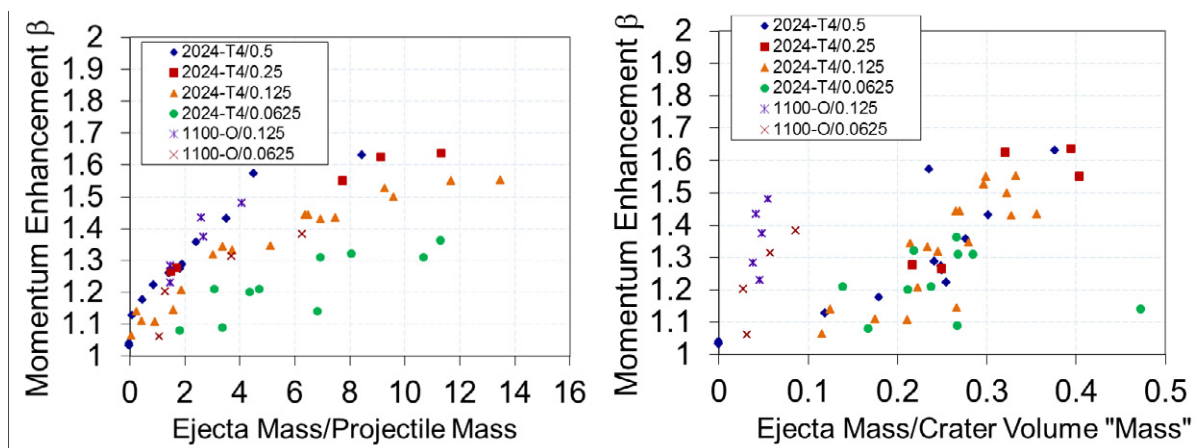

Fig. 9. Momentum enhancement β in terms of ejecta mass normalized by projectile mass (left) and displaced mass in the crater volume (right) for the aluminum striking aluminum (data from [8]), the left image still showing a size scale effect rather than a direct correlation with ejecta mass. Legend shows target material alloy/aluminum projectile diameter in inches.

As described in Ref. [5], we combined the Denardo and Nysmith data in [7,8] looking at both the scale size effect and the effect of ρ (the density of the impactor). In their original report they had used a curve fit directly to β. However, in our analysis we felt the main focus was on the amount of momentum due to the ejecta, so we focused on $\beta - 1$, the amount of momentum in the target above that of the projectile. When the analysis of the aluminum-target data is performed with

$$\beta(v) - 1 = (\rho / \rho_{ref})^a (D / D_{ref})^b (\beta_{ref}(v) - 1), \tag{1}$$

a good fit for the aluminum data is $b = 0.4$ and $a = 0.5$. When the data in Fig. 5 is plotted to reduce the various terms to the same curve, i.e., the inverse of the data fit equation, or

$$\beta^*(v) - 1 = (\rho / \rho_{ref})^{-a} (D / D_{ref})^{-b} (\beta(v) - 1), \tag{2}$$

it is seen that the stronger aluminum targets as well as the rock targets fall onto (different) straight lines, shown in Fig. 10. These straight lines, determined by least squares using all 6 rock data points and 70 Al-2024 target points (all save the polyethylene impacts below 1 km/s where elastic rebound increased β), are indicated by dot-dashed lines in the figure. They provide the following momentum enhancement predictions,

2024 Aluminum Target: $\qquad \beta(v) - 1 = (\rho / \rho_{ref})^{0.5} (D / D_{ref})^{0.4} (0.179v - 0.105),$ (3)

Rock Target: $\qquad \beta(v) - 1 = (\rho / \rho_{ref})^{0.5} (D / D_{ref})^{0.4} (0.851v - 0.866).$ (4)

Impact speeds v are in km/s; ρ is the impactor density. The reference values for the impactor are $\rho_{ref} = 2.78$ g/cm^3 and $D_{ref} = 1.27$ cm, and the β_{ref} curves for the targets are, for 2024, $\beta_{ref} = 0.179v + 0.895$, which has a $\beta = 1$ intercept at 0.585 km/s, and for rock $\beta_{ref} = 0.851v + 0.134$, which has a $\beta = 1$ intercept at 1.017 km/s. Based on computational results in Ref. [9] described below, the impactor density value used in these equations should not exceed ρ_{ref}, or that $(\rho/\rho_{ref})^{0.5}$ should be replaced with $\min(1, (\rho/\rho_{ref})^{0.5})$ in Eqs. (3) and (4). The 2024 aluminum target curve is based on data from 1 to 8 km/s and the rock curve is based on data from 2 to 4.5 km/s. Given this analysis, our rock impacts are in line with the previous rock data, implying that the impact behavior of our tests is in line with the previous data which shows scaling effects and impactor density effects. It is conceivable that the scale size saturates, just as the density term saturates. This point is discussed in Ref. [5].
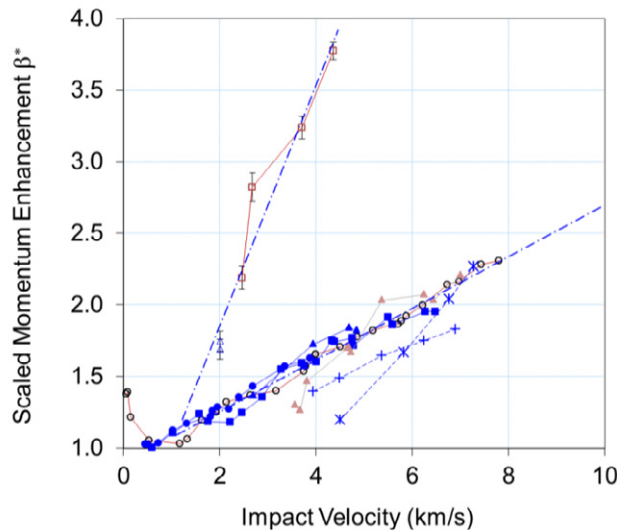

Fig. 10. Experimental results for scaled momentum enhancement β^*, scaled to $\rho_{ref} = 2.78$ g/cm^3 and $D_{ref} = 1.27$ cm using $a = 0.5$ and $b = 0.4$, for all data in Fig.5. The 2024-T4 aluminum targets and the rock targets all lie on a (different) line, and the least squares fit is shown. In particular, the two new data points (at $v = 2$ km/s, $\beta^* \approx 1.75$) agree with the scaling analysis. The legend for Fig. 10 is the same as in Fig. 5.

3. Computational Results on Momentum Enhancement and Damage Size Scaling

The first two authors did an extensive exploration of momentum enhancement through large-scale numerical simulations that were presented at the 2010 Hypervelocity Impact Symposium in Freiburg, Germany [9]. Computations were performed with CTH for impactors shaped as spheres, flat plates, and hollow cylinders. Impactor materials included lithium, polyethylene, aluminum, copper and tungsten with densities 0.53, 0.915, 2.79, 8.93, and 19.2 g/cm³, respectively. Impacted (target) materials included water ice, aluminum, a lunar-based rock, and granite with various degrees of porosity, where densities ranged from 0.914 to 2.79 g/cm³. In addition, the fracture properties of the target material were varied with fracture strengths ranging from 1 MPa to 1 GPa. Qualitative conclusions of these numerical studies were that momentum enhancement is expected to be greatest when

1. The impactor shape is close to that of a sphere,
2. The impactor density and target density are similar,
3. The target has a low tensile fracture stress,
4. The target has little porosity.

In an asteroid or comet nucleus deflection scenario, we have control over the first two, but not the second two. It is likely that the celestial object will have a low tensile fracture stress, but the porosity is an open question.

These computations were performed at the centimeter scale for the impactor, but the only scale effect in these computations is an increase in material strength with an increase in strain rate and the fact that there is a computational scale for mesh resolution. The strain-rate strengthening does not produce a large enough change in result to be the cause of the observed scale effect. Our current computations are not able to reproduce the scale effect observed in the aluminum computations. Computational models for other deflection techniques based on material supplied by the deflected body will presumably have similar difficulties, since the quantitative amount of momentum enhancement is due to cratering, which is controlled by material fracture and failure properties and can occur over an extended time.

To find a relationship between the implicit damage size by linking experimental momentum enhancement and computational damage modeling, consider the following argument. We first use a simple damage model and describe its effect on momentum enhancement. This damage model has shown good results, as described in the next paragraph. Then the momentum enhancement from experiments will be tied to these computations.

The first two authors computationally explored the interesting result (described in the previous section) for the aluminum targets that the stronger aluminum (2024-T4) had smaller craters but more momentum enhancement than did the weaker aluminum (1100-O). The computations agreed with the experiments in that the weaker aluminum had the larger craters and also that there was no scale-size effect for the crater extent – i.e., experimentally it was observed that there was little influence of impactor size on P/D_p and D_c/D_p, where P is the depth of the crater, D_c is the diameter of the crater, and D_p is the diameter of the impactor [10]. Since the computations showed little scale effect due to the plasticity model, prompted by earlier work in target perforation [11] it was decided to explore the influence of a failure model. A simple failure model was introduced where the material was assumed to fail when the equivalent plastic strain ε_p reached a predetermined failure strain ε_f. When the equivalent plastic strain reached this failure strain, material strength was removed so that the material could no longer support shear stresses or tensile loads. A parameter study was performed using material properties for Al 2024-T351 as the target for impacts of spheres at 8 km/s, with the results and a curve fit shown in Fig. 11. The curve in the graph is given by $\beta - 1 = 1.2(\varepsilon_f)^{-0.6}$, though exponents ranging from -0.6 to -0.5 give reasonable agreement with the computational points.

The large range of failure strains are reasonable. Bao and Wierzbicki report a failure strain of 0.45 for Al 2024-T351 [12]. Using the flow stress $Y(\varepsilon_p)$ of Al 2024-T351 as given in Johnson [13], the work per unit volume to failure is

$$W = \int_0^{\varepsilon_f} Y(\varepsilon_p)\, d\varepsilon_p = \text{constant} = 263\text{MPa}. \tag{5}$$

When the flow stress for for Al 1100-O as given in Johnson [13] is used, assuming a constant failure work, the computed failure strain for Al 1100-O is 1.50. This difference in failure strain, while using the appropriate flow stress, led to a similar momentum transfer to that seen in experiment after the same size scaling was applied to both. In particular, the stronger 2024 material had more momentum transfer in a quantitative amount compared to the weaker 1100 material [10]. Thus, this failure model is a reasonable approach

We now link the relationship between failure strain and momentum enhancement in Fig. 11 with the relationship between scale and momentum enhancement in Eq. (3) for Al 2024. At 8 km/s, Eqs. (3) and $\beta - 1 = 1.2(\varepsilon_f)^{-0.6}$ combine to give

$$\varepsilon_f \sim (D_{ref}/D)^{2/3}. \tag{6}$$

Thus, a damage model with a length scale in it would be expected to exhibit this sort of behavior (to the -2/3 power) in the failure strain as a function of the scale size.
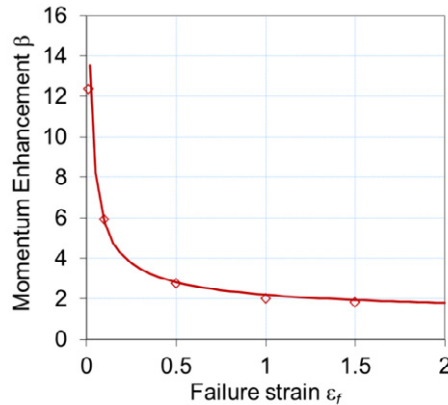
Fig. 11. Results of CTH computations using the 2024-T351 flow stress constitutive model for the target showing the effect of failure strain on momentum enhancement of 1-cm diameter Al 6061-T6 projectile strikes at 8 km/s.

4. Conclusions

In conclusion, we have experimentally shown for relatively large impactors momentum enhancements of $\beta = 2.1 – 2.2$ for aluminum spheres striking granite at 2 km/s, and we have, through analysis, shown that these results are in line with available data, and in particular that they imply a size scale effect based on the impactor size. The scale-size effect on the momentum enhancement is extremely important in the application of deflecting an asteroid. The relationship between a damage measure (failure strain) and scale size was described, exhibiting an exponent of -2/3.

Acknowledgments

References

[1] K. A. Holsapple, About deflecting asteroids and comets, in: M. J. S. Belton, T. H. Morgan, N. H. Samarasinha, D. K. Yeomans (Eds.), *Mitigation of Hazardous Comets and Asteroids,* Cambridge Univ. Press, Cambridge, 2004, pp. 113-140.
[2] NASA, Near-earth object survey and deflection: analysis of alternatives. Report to Congress, March 2007, available at http://www.nasa.gov/pdf/171331main_NEO_report_march07.pdf and http://neo.jpl.nasa.gov/neo/report2007.html.
[3] NASA. 2006 near-Earth object survey and deflection study (draft pre-decisional material), available at http://www.hq.nasa.gov/office/pao/FOIA/NEO_Analysis_Doc.pdf and http://neo.jpl.nasa.gov/neo/report2007.html.
[4] National Research Council, Defending planet Earth: Near-Earth object surveys and hazard mitigation strategies: final report, National Academies Press, Washington, D.C., 2010.
[5] J. D. Walker, S. Chocron, D. D. Durda, D. J. Grosch, N. Movshovitz, D. C. Richardson, E. Asphaug, Momentum Enhancement from Aluminum Striking Granite and the Scale Size Effect,*submitted to IJIE, 2012.*
[6] M. Yanagisawa, S. Hasegawa, Momentum transfer in oblique impacts: implications for asteroid rotations, *Icarus,* **146** (2000) 270-288.
[7] B. P. Denardo, Measurements of momentum transfer from plastic projectiles to massive aluminum targets at speeds up to 25600 ft/s, NASA Technical Note D-1210, 1962.
[8] B. P. Denardo, C. R. Nysmith, Momentum transfer and cratering phenomena associated with the impact of aluminum spheres into thick aluminum targets at velocities to 24000 ft/s, in: *Proceeding of the AGARD-NATO Specialists*, Vol. 1: The Fluid Dynamic Aspects of Space Flight, Gordon and Breach Science Publishers, New York, 1964, pp. 389-402.
[9] J. D. Walker, S. Chocron, Momentum enhancement in hypervelocity impact, *Int. J. Impact Engng,* **38** (2011) A1-A7, doi:10.1016/j.ijimpeng.2010.10.026.
[10] J. D. Walker, S. Chocron, Role of target strength in momentum enhancement, in: M. L. Elert, W. T. Buttler, J. P. Borg, J. L. Jordan, T. J. Vogler (Eds.), Shock Compression of Condensed Matter-2011, AIP Press, Melville, NY, 2012, pp. 1019-1022.
[11] C. E. Anderson, Jr., V. Hohler, J. D. Walker, and A. J. Stilp, The influence of projectile hardness on ballistic performance, *Int. J. Impact Eng.* **22** (1999) 619-632.
[12] Y, Bao and T. Wierzbicki, A comparative study on various ductile crack formation criteria, *J. Eng. Mat. Tech.* **126** (2004) 314-324.
[13] G. R. Johnson, Material characterization for warhead computations, in: J. Carleone (Ed.), *Tactical Missile Warheads,* American Institute of Aeronautics and Astronautics, Washington, D. C., 1993, pp. 165-197.